"INDUCED POLARIZATION DATA AT ROOSEVELT HOT SPRINGS GEOTHERMAL AREA, UTAH"

by

Jean J. Chu
Stanley H. Ward
William R. Sill
John A. Stodt

Paper presented at the 49th Annual International SEG Meeting, November 4-8, 1979, in New Orleans

ABSTRACT

Both field and laboratory broadband multispectral data have been gathered in a study of IP phenomena at the Roosevelt Hot Springs geothermal area. The field survey involved two traverses across the main part of the present day hydrothermal system. The laboratory research gathered data at 25°C, 50°C, and 75°C, on hydrothermally altered rocks from the hot springs area.

Laboratory data indicate a small IP effect of 3 to 23 mr at low frequencies (0.004 Hz). High frequency (10^3 Hz) IP data ranged from 20 to 100 mr. The IP effect is frequency dependent, and is not affected markedly by moderate changes in temperature; it is also dependent upon the quantities of pyrite and clay minerals. Pyrite affects the phase spectrum well above 1 Hz, and its effect is different from that of polarizable clays.

The field data at the higher frequencies show both positive and negative phase values, which can be explained by electromagnetic coupling. Extrapolated phase data reveal a small anomalous region of 20 to 34 mr along one of the profiles; the majority of the data ranged from 7 to 15 mr.

The laboratory and field data indicate only a small IP effect over the hydrothermal system; it could be considered as background and hence of no consequence. There seems to be no large scale delineation of the geothermal field.

INTRODUCTION

The purpose of this study was to investigate the usefulness of conducting an induced polarization (IP) survey in a geothermal environment of the high temperature convective hydrothermal type. Can one utilize the polarization characteristics of clays and pyrite to distinguish zones of low resistivity due to hydrothermal alteration from those due solely to the presence of hot brines?

Risk (1975), in a resistivity survey of the Broadlands geothermal field, New Zealand, briefly mentioned detection of an IP anomaly, suggesting its probable cause as disseminated sulfide minerals. Induced polarization surveys over geothermal systems have been conducted by Zohdy et al (1973), and Ross (1979). The former employed a pole-dipole array, using 0.1 Hz and 1.0 Hz, while the latter used the dipole-dipole array with measurements taken in the time domain. In both cases, IP anomalies were recorded: Zohdy et al (1973), working in the Mud Volcano area of Yellowstone National Park, cited the relatively high concentrations of pyrite as the probable cause of the anomalies; Ross (1979) stated that the polarization data gathered in the Cove Fort - Sulphurdale thermal area, Utah, were too limited to speculate on the net polarization characteristics due to pyrite, clay and zeolite mineralization. These surveys indicated the need for documented study of IP phenomena in geothermal areas. It was to fulfill this need that broadband multispectral data were gathered both in the field and in the

laboratory during the years of 1978 and 1979.

The geothermal system chosen for this study was the Roosevelt Hot Springs Known Geothermal Resource Area (KGRA) (Figure 1). This area contains a structurally controlled, hot-water dominated system in plutonic and metamorphic rock (Nielson et al, 1978). Detailed geological, geochemical and geophysical work has led to the development of a complete case study of the area (Ward et al, 1978). Extensive electrical data have been gathered involving 100 m, 300 m, and 1 km dipole-dipole resistivity, Schlumberger resistivity, electromagnetic, and magnetotelluric soundings. In addition, controlled source audio-magnetotelluric, bipole-dipole resistivity, telluric ratio, and self-potential surveys have been conducted. The geology of the area is summarized by Ward et al (1978); detailed geology is given by Nielson et al (1978). Research in this region continues to the present.

Induced polarization in the frequency domain is a phenomenon whereby resistivity changes as a function of frequency. This effect is produced by the presence of clays, zeolites, conductive oxides and conductive sulfides. In the Roosevelt Hot Springs thermal area, extensive hydrothermal alteration has produced clays, pyrite and marcasite (Parry et al, 1978; Ballantyne and Parry, 1978). A monitoring of the IP phenomena due to these alteration minerals might allow us to map the zones of alteration. Our study was conducted to assess this possibility.

We present our results in three sections. Laboratory data are given first, with schematic explanations of the possible reasons behind the IP behavior of hydrothermally altered rocks. Data from the field survey follow, and we discuss the methods available to remove inductive

FIG. 1. Location map of Roosevelt Hot Springs KGRA. Base line, heat flow (mW/m^2) and apparent resistivity (Ω-m) contours from Ward et al (1978). IP traverses with dipole-dipole array shown as Lines 1 and 2. Productive wells shown by solid dots, "dry wells" by open circles. Cores for laboratory research taken from three shallow alteration holes shown by circles with crosses. Hachured region is bedrock exposure of Mineral Mountains; white area is quaternary alluvium; black areas are quaternary sinter deposits and altered rock. The area of highest heat flow is shaded. The Opal Mound Fault is shown.

CHU
Fig. 1

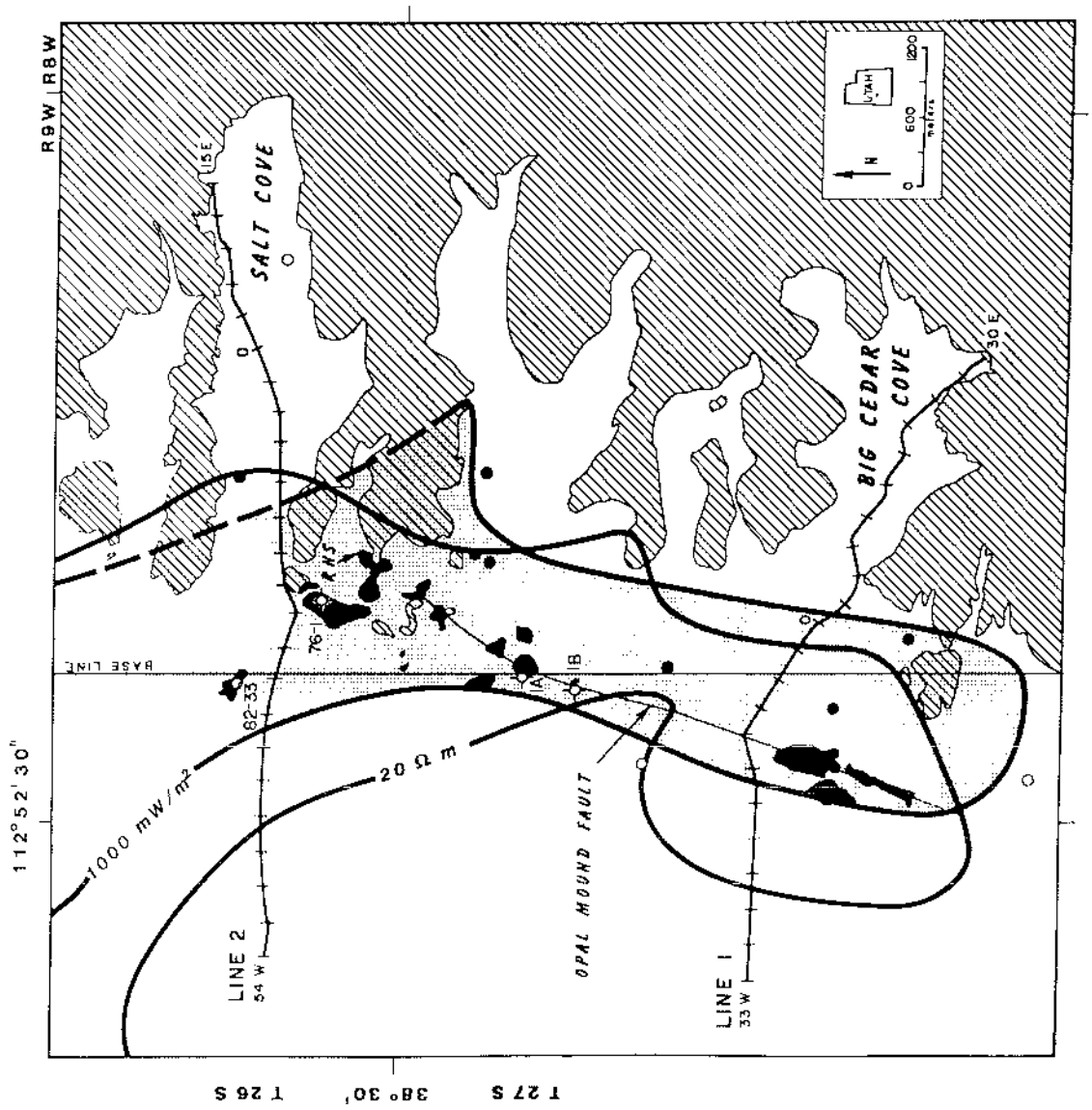
R9W R8W
SALT COVE
BIG CEDAR COVE
BASE LINE
1000 mW/m²
20 Ω m
OPAL MOUND FAULT
LINE 2
54 W
LINE 1
33 W
82-33
76-1
A
B
UTAH
600
1200
miles
112°52'30"
38°30'
T 27 S
T 26 S

electromagnetic (EM) coupling from the field measurements. In the final section, we summarize and integrate the essentials from the laboratory and field data, and draw conclusions.

LABORATORY RESEARCH

Data Acquisition

Parry et al (1980) analyzed the subsurface alteration in three shallow diamond drill holes (maximum depth: 70m) located near the Opal Mound Fault (Figure 1). On the basis of their data, core samples were selected covering the spectrum of low to high clay and pyrite content.

Sample preparation. - The cores were 4.7cm in diameter with lengths varying from 4.8cm to 7.2cm. Most of the altered samples were friable, consequently, each core sample was enclosed in epoxy. The epoxy itself showed no significant IP effects.

Expansion and cracking of the sample holders were avoided by soaking those rocks with montmorillonite content greater than 10 weight percent in distilled water prior to complete enclosure in the epoxy. Holes were drilled into the ends of the enclosed samples. They were then vacuum saturated with 0.1 N NaCl solution, which is approximately the same concentration as the brine encountered in the Roosevelt Hot Springs thermal area (Parry et al, 1978).

Apparatus and experimental procedure. - A phase-sensitive receiver (ZERO, GDP-12/2G) was employed as both a digital voltmeter and a signal generator. A chart recorder monitored any erratic or drifting behavior of the experimental apparatus. To maintain constant temperature, the

sample was placed in an oven, and resistors used in the measurement procedure were enclosed in an insulated container. A four electrode arrangement was utilized with Ag-AgCl electrodes. A common ground was established, and calibration of the receiver was conducted at the same time measurements were being taken. Measurements were stacked to suppress noise; the stacking ranged from 4096 stacks at 1024Hz, down to 16 stacks at 1/256Hz. Laboratory data were obtained at all the frequencies used in the field, with an additional six frequencies up to 1024Hz. The complex resistivity for each sample was measured in this sequence: at 25°C, 50°C, 75°C, and again at 25°C. The repeat room temperature measurement was made to ensure reproducible results. The temperature range was chosen to reflect the environment of the shallow alteration hole 1A (Sill and Bodell, 1977; Figure 1).

Current densities were ordinarily kept well below 1.0 $\mu amp/cm^2$. Any sample with current densities greater than 1.0 $\mu amp/cm^2$ was monitored for non-linear behavior by measuring the harmonic content of the voltage signal. In all cases the higher harmonics had amplitudes at least one thousand times smaller than the fundamental, i.e. no significant non-linear effects were recorded.

Determination of parameters. - The IP behavior of the core samples largely depended upon three parameters: porosity, the resistivity of the pore fluid, and the clay and pyrite content. The resistivity of the electrolyte was closely monitored. The pyrite content, in weight percent, was based upon the analyses done by Parry et al (1978).

Clay content is given by the Qv value, which is the effective concentration of clay-exchange cations (equiv/liter or meq/ml) in the

pore solution. This value is thought to reflect the contribution of clays to the IP effect. Qv can be determined independently from the ratio of cation exchange capacity of the core sample (meq) to the pore volume of the sample (ml). The cation exchange capacity, CEC, in meq per 100gm of the rock sample, was measured by atomic absorption spectrometry. A summary of the measurements is given in Table 1.

Both Qv and porosity depend upon the volume of interconnected pore passages within the rock. For non-expanding core samples, the pore volume was taken to be the volume of water absorbed by the rock after the two to three month soaking period. For samples which expanded [(c) and (f) of Table 1], the pore volume was assumed to be the difference between the volume of water absorbed and the change in volume of the core sample. This latter procedure may have resulted in inflated Qv values; but if the former procedure had been followed, the Qv values for the expanded samples (c) and (f) would have been 1.34 equiv/l and 2.22 equiv/l respectively, which are still larger than the Qv values for the non-expanded samples.

The porosity (effective porosity) was determined from the ratio of the pore volume of the sample to the volume of the rock when wet.

Data Interpretation

Ten samples were prepared. Two of the samples were slightly hydrothermally altered, while another two were inadequately encapsulated. The remaining six samples were highly altered, and the data for these are shown in Table 1 and Figures 2a-2f.

Effects of temperature. - The resistivity of the altered rocks is

TABLE 1. Parameter values of effective porosity, cation exchange capacity (CEC), clay (Qv) and pyrite content, for six core samples identified by drill hole and depth of recovery. Labels a-f relate samples to spectra shown in Figures 2a-2f. Range in IP effect taken from data at 25°C. Resistivity obtained at room temperature using 1/256Hz.

CHU
Table 1

Sample	Resistivity (Ω-m)	IP effect (mr)	Porosity	CEC (meq/100 gm)	Qv (equiv/l)	Pyrite (wt.%)
(a) [76-1] 30.8m	11.5	7-20	0.33	4	0.22	0.2
(b) 1A 37.5m	5.2	12-37	0.30	19	1.23	1.0
(c) 1A 49.7m	3.8	12-25	0.20	35	3.2	2.4
(d) 1A 58.5m	6.6	9-92	0.36	8	0.46	4.3
(e) 1A 61.3m	7.1	11-100	0.28	15	1.22	8.6
(f) 1A 51.2m	3.4	7-23	0.15	52	6.2	9.1

FIGS. 2a-2f. Laboratory data arranged in increasing pyrite content, for frequency range 1/256 Hz to 1024 Hz. Electrolyte is 0.1 N NaCl. For resistivity plot, lower 25°C curve taken after sample cooled from 75°C; data for rocks where 25°C curves differed by less than 0.3 Ω-m have been combined. Sample (c) heated to 50°C only. For phase plot, double set of data at 25°C averaged (solid dots); vertical lines and open circles represent 50°C and 75°C range in values. Horizontal bar graphs represent polarizable clay (Qv) and pyrite content.

CHU
Figs 2a-2f

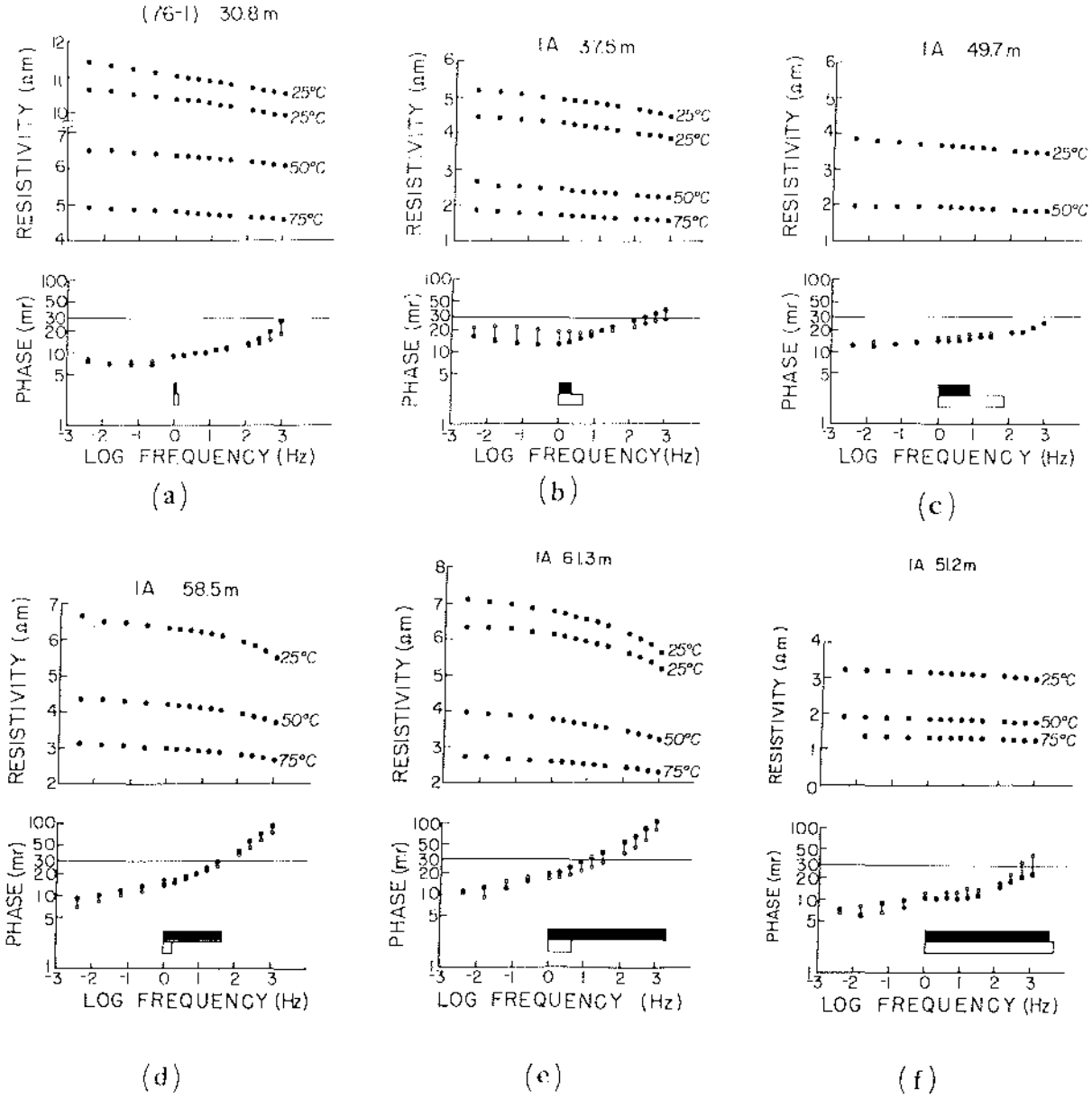

determined by rock porosity, the electrical properties of the pore fluid and the clay and pyrite content. In this study, the resistivity of the electrolyte is set and monitored, leaving porosity, and clay and pyrite content as variable factors. The influence of porosity alone is expressed by Archie's Law, while that including the contribution of clay can be found in an expression developed by Waxman and Smits (1968). Temperature dependent forms of these two expressions can be obtained by referring to Keller and Frischknecht (1966, p. 31), and Waxman and Thomas (1974).

We found that core samples with high Qv values [(c) and (f) of Table 1] behaved according to the Waxman-Smits model, while those with lower Qv values [(a), (d), and (e) of Table 1] had resistivities which followed Archie's Law. By varying the porosity exponent, we can fit the data for sample (b) using either Archie's Law or the Waxman-Smits model.

The effect of temperature on resistivity and phase spectra is shown in Figures 2a-2f. Rock resistivities change as a function of temperature according to the above two models. The phase spectra show small changes in character as temperature is increased. At the highest frequencies, the phase values drop by 10 to as much as 22 milliradians in Figures 2a, 2b, 2d, and 2e. For eight of the ten samples measured, phase values at the lower frequencies did not change by more than 4mr as the temperature was increased; for two samples, a phase change of 8mr occurred from 25°C to 75°C.

Effects of Frequency. - Figures 2a-2f illustrate the frequency dependence of the hydrothermally altered core samples. As frequency increased, the greatest change in the phase curves occurs in samples (d)

and (e). Both samples have comparatively high pyrite content and relatively low Qv values. The behavior of their respective resistivity curves follow the observations made by DeWitt (1978) and Wong (1979); as the metallic content in a rock increases, the IP effect increases.

We now examine the phase spectra behavior of the laboratory data at and below 32Hz, i.e. the frequency range used in the field survey. For the samples (c) and (f), which have very high Qv values, the phase spectra are approximately independent of frequency. Samples (b), (d), and (e) exhibit a definite frequency dependence in the phase curves, even to the lowest frequency. Sample (a), which is low in both pyrite and Qv value, has a flat phase spectrum. However, the phase spectrum of another sample (not shown here) with similar low pyrite and clay content (room temperature resistivity: 50Ω-m) shows a smooth drop in phase values from 12mr to 3mr over the frequency range of 1/4Hz to 1/256 Hz. For yet another sample (also not shown) the phase value changes from 14mr at 1Hz, to 11mr at 1/16Hz, and finally to 17mr at 1/256Hz. Such data were reproducible, and well above the measurement noise level for these samples. Thus, hydrothermally altered rocks can exhibit IP effects that are frequency dependent at low frequencies.

In closing, for the entire suite of ten samples, the phase values recorded at the lowest frequency varied from 3mr to 23mr. At the highest frequency of 1024Hz, phase values ranged from 20 to 100mr.

The effect of clays and pyrite on phase spectra. - Previous laboratory measurements (Tripp, pers. com.) on altered material have shown low frequency (<1Hz) phase anomalies, which have been attributed to the effect of pyrite; higher frequency (>1Hz) polarization is thought

to be due to the presence of clays and fine grained material (DeWitt, 1978). We can assess the validity of this hypothesis by an examination of the laboratory phase data (solid dots) shown in Figure 2a-2f. We first examine the phase spectra with respect to pyrite content: spectra (a) through (f) have been arranged according to increasing pyrite content, as shown by the bar graphs. We note an abrupt change in spectrum character when the pyrite content is about 3% (c and d). Another change occurs between (e) and (f). With the exception of samples (c) and (f), the maximum measured phase increases with increasing pyrite content. In contrast, examination of the spectra in terms of increasing Qv values (bar graphs) shows no obvious trends.

The various effects of clay and pyrite can be explained by consideration of the IP models proposed by DeWitt (1978) and Wong (1979). Both models give similar results but the parameters of DeWitt's model are more useful in the discussion that follows.

The model of DeWitt (1978) predicts that the maximum phase angle occurs at the frequency

$$f_m = \left[\sqrt{(2+v)/2(1+2v)}\ A/\rho_1 a\right]^{1/2} / 2\pi \qquad (1)$$

and that the maximum phase at this frequency is

$$\tan \phi_m \propto 9v/[(1+2v)(2+v)]\sin \pi/2\, C \qquad (2)$$

where

v = volume fraction of polarizable spheres,

a = radius of polarizable spheres,

ρ_1 = background (rock) resistivity,

A = magnitude of the surface impedance at W = 1, and

C = frequency dependence of the surface impedance

(C = .5 for diffusion and C = 1.0 for charge separation).

The model predicts that the frequency at which the peak of the phase dispersion occurs depends mainly on the background resistivity (ρ_1) and the grain size (a), since the magnitude (A) and the frequency dependence (C) of the surface impedance are relatively constant for a given polarizable material. The maximum phase, on the other hand, depends mainly on the volume fraction of the polarizable material present. These models have been developed specifically for conducting spheres but they might be expected to indicate the general trends for clay polarization as well. The grain size of the pyrite particles was determined by optical examination in reflected light of polished sections taken from drill holes 76-1 and 1A (Figure 1). The average size was found to be 0.06mm with a standard deviation of .02mm. The size of clay minerals tends to be less than about 2μ (Grim, 1968). If we assume that the above models work not only for conductive minerals but for any polarizable material, we can expect on the basis of grain size alone that the maximum phase for clays will appear at a higher frequency than that for pyrite.

Putting the mean grain size of the pyrite into equation 1 and using the sample resistivities and A = 2Ωm^2, C = 0.65, the frequency of maximum phase is typically found to be above 1KHz. Thus in the sample measurements, the measured phases are probably due to contributions from clay and pyrite, both of which have dispersion peaks above the frequency

window of the laboratory measurements.

There is evidence to justify placing the phase spectrum peak of the clay and pyrite grain size groups above 1024Hz. Hallof et al (1979), in describing massive sulfide mineralization, indicated peaks well above 3Hz. DeWitt (1978) recorded measurements on two core samples from the Tyrone prophyry copper deposit near Silver City, New Mexico, and compared his data with some in situ IP measurements made at the same deposit by Pelton et al (1978). He found that the dispersion related to the sulfide response was reasonably separated from a higher frequency dispersion whose peak was above 10^5Hz, which he attributed to membrane polarization of alteration minerals. Finally, Tripp (1977), gathered data up to 10^5Hz on core samples from the shallow alteration holes 1A and 1B (Figure 1). The spectra showed a steady upward trend in phase values, similar to the phase curves of Figures 2a-2f. Most of his IP data indicated peaks well above 10^5Hz. However, one of his samples showed a phase dispersion peak at approximately $5x10^3$Hz (Pelton, 1977, p. 113), which could be attributed to possible pyrite mineralization (Tripp, per. com.).

A possible explanation for the changes in the phase spectra between Figures 2b and 2e is shown in Figure 3. Since the polarizable clay content, expressed as Qv, is essentially the same for these samples, the clay dispersion as shown in Figure 3 is the same for both samples. Increasing the pyrite content causes an increase in the phase curve as shown in the sketch.

The change in spectra between samples (e) and (f) (Figures 2e and 2f) might be the result of the effects shown in Figure 4. In this case

FIG. 3. A schematic explanation of phase spectra in Figures 2b and 2e, based on conclusions from DeWitt (1978) and Wong (1979). Bottom curves represent spectral dispersions associated with clay and pyrite grain size groups; clay dispersion is fixed. Summation of respective dispersion curves shown in upper diagram; sketch of laboratory data drawn with solid lines.

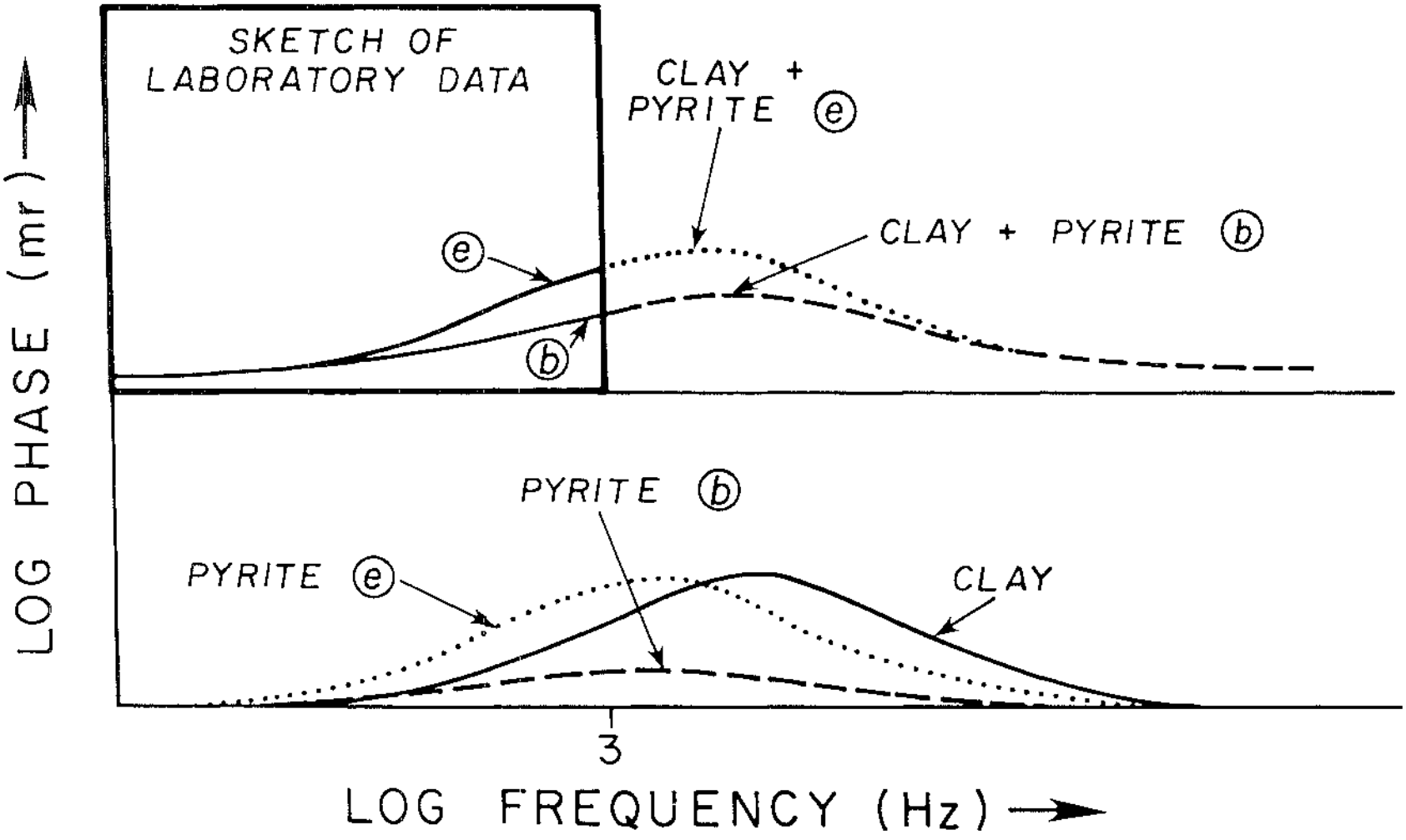
SKETCH OF
LABORATORY DATA
CLAY +
PYRITE (e)
CLAY + PYRITE (b)
(e)
(b)
PYRITE (b)
PYRITE (e)
CLAY
3
LOG PHASE (mr)
LOG FREQUENCY (Hz)

CHW
Fig. 3

FIG. 4. A schematic explanation of phase spectra shown in Figures 2e, 2f, based on studies by DeWitt (1978) and Wong (1979). Bottom curves represent spectral dispersions associated with clay and pyrite grain size groups. Summation of respective dispersion curves shown in upper diagram; sketch of laboratory data drawn with solid lines.

CHU
Fig. 4

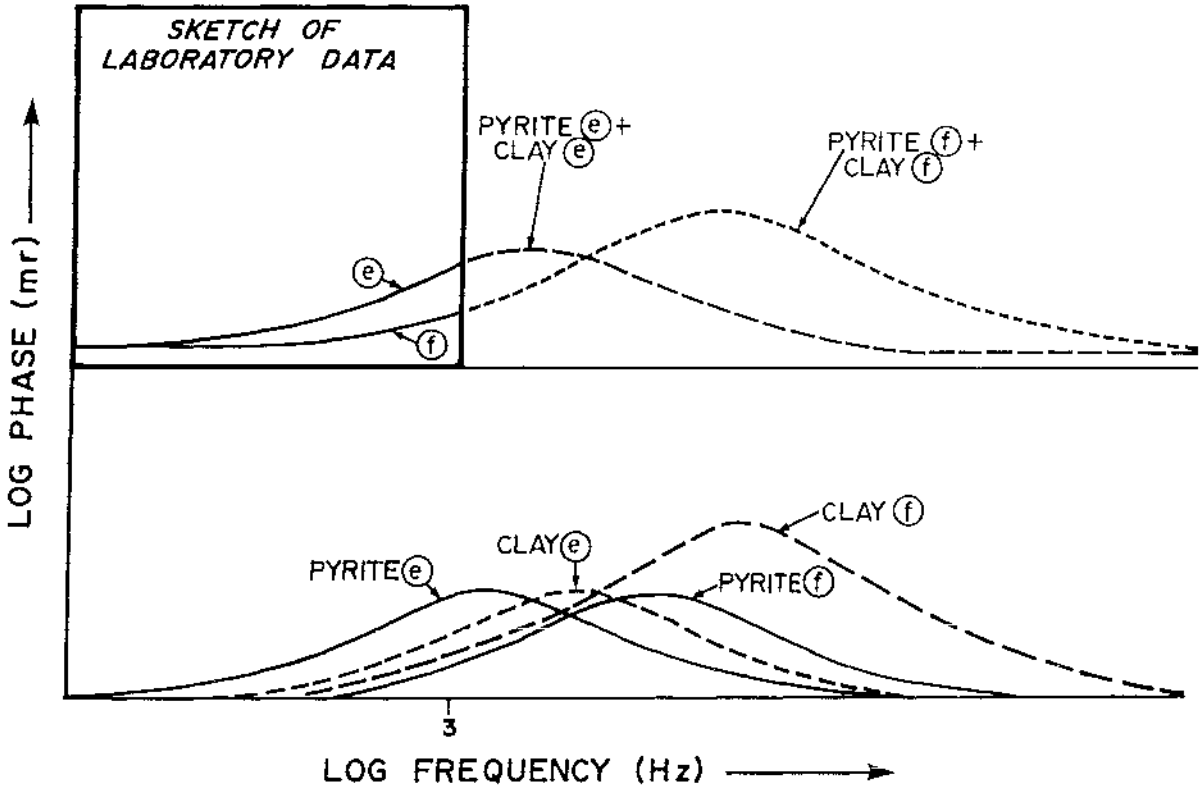
SKETCH OF
LABORATORY DATA
PYRITE (e) +
CLAY (e)
PYRITE (f) +
CLAY (f)
(e)
(f)
LOG PHASE (mr)
CLAY (f)
CLAY (e)
PYRITE (e)
PYRITE (f)
3
LOG FREQUENCY (Hz)

the pyrite contents are about the same but the clay content (Qv) of sample (f) is larger. The increased clay content has lowered the background resistivity of sample (f) and according to equation (1) the pyrite and clay dispersions, labelled "PYRITE f" and "CLAY f" respectively, have been moved to higher frequencies. Summing up the effects as in the top of the figure gives a sketch of the observed data.

The lowering of the background resistivity as temperature increases might also be expected to shift the phase dispersions of our samples. As noted previously, for samples (a), (b), (d), and (e), there is a noticeable drop of as much as 22mr in the magnitude of the phase values at the highest frequencies. This may be due to the fact that as temperature increases, the resistivity of the rock sample decreases; the phase spectrum of the rock will shift slightly up frequency, as shown schematically in Figure 5. In the frequency range of the lab data, this shift is perceived as a drop in phase values for the positive slope of the phase spectrum, and an increase in phase values for the negative slope of the spectrum (see phase spectra in Figures 2b and 2d). Figure 5 also shows that one may be able to gain more information on low frequency phase behavior by increasing temperature. An exception to the above sample (f) of Figure 2f, which behaves in an opposite manner at the higher frequencies: the phase rises by about 20mr at 75°C.

FIG. 5. Schematic explanation of temperature effect on phase spectrum for sample (b) of Figure 2b. Heavy lines denote frequency range of lab data. The drop in resistivity as temperature rises, shown by the resistivity plot, causes the phase spectrum to shift to a higher frequency; thus one may be able to gain more information on the phase behavior at low frequencies by increasing temperature.

CHU
Fig. 5

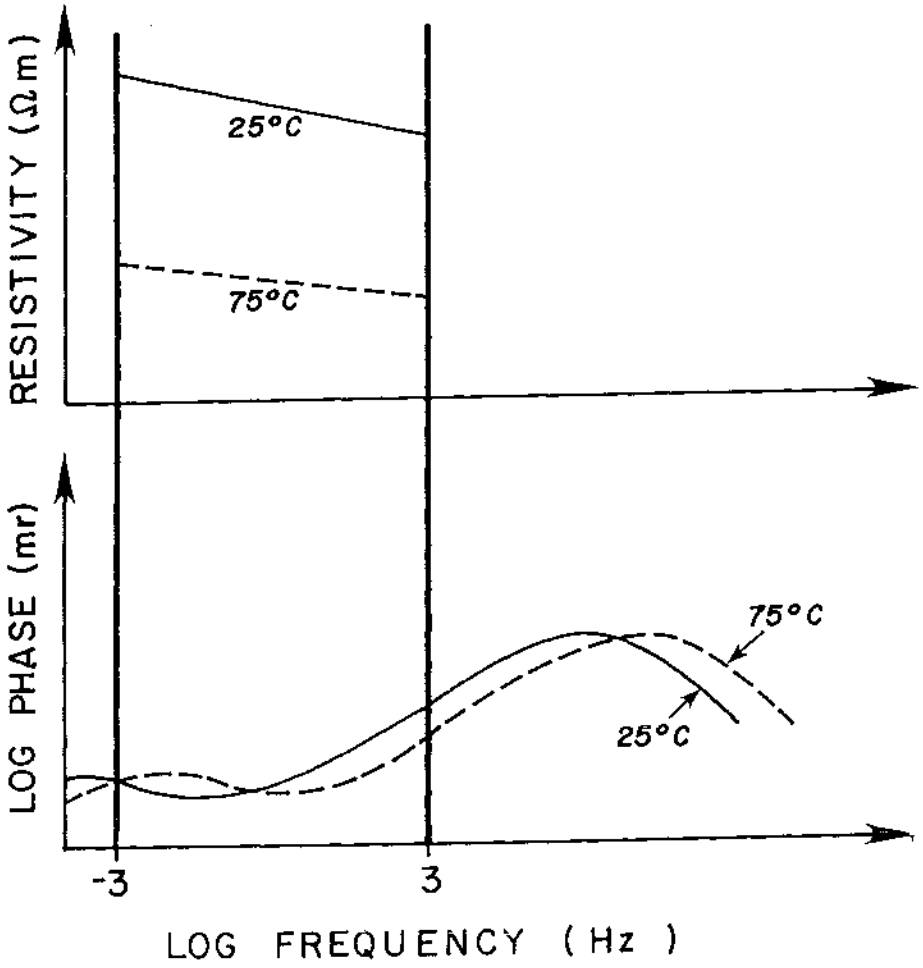
RESISTIVITY (Ωm)
25°C
75°C
LOG PHASE (mr)
75°C
25°C
-3
3
LOG FREQUENCY (Hz)

FIELD SURVEY

Data Acquisition

During the summer of 1978, 15 line-km of multi-frequency IP data were obtained across the Roosevelt Hot Springs geothermal system, along the two profiles shown in Figure 1. Line 1 crosses the southern half of the geothermal system while Line 2 crosses the northern portion. The zone of maximum hydrothermal alteration (Parry et al, 1980) is situated between Lines 1 and 2. However, permit restrictions limited the traverses to roadways only, and hence the location and configuration of the profile lines. The western ends of Lines 1 and 2 correspond to 2200 N and 5950 N, respectively, of the dipole-dipole resistivity survey grid established by Ward and Sill (1976); the base line of this grid is also shown in Figure 1.

Drill hole data revealed that polarizable clays were primarily confined to the upper portion of the holes (Ballantyne and Parry, 1978: Rohrs and Parry, 1978; Ballantyne, 1978). The depth of K-feldspar stability was estimated at 400m (Ward and Sill, 1976). To resolve zones of possible alteration, we used the collinear dipole-dipole array, with dipole lengths of 100m and 300m and maximum n spacings of 4 and 6, respectively.

The equipment used in the survey included the ZERO phase-sensitive receiver (GDP-12/2G), a Geotronics FT20A transmitter and a motor

FIG. 9. 2D resistivity model (bottom) for Line 2. Contoured apparent resistivity data (top) obtained at 1/256 Hz with 300 m dipoles. Contour and model pattern codes same as in Figure 8. Resistivity of model blocks in Ω-m. Based on Figure 10, faults exposed at the surface are indicated by "f"; inferred faults shown with " ?".

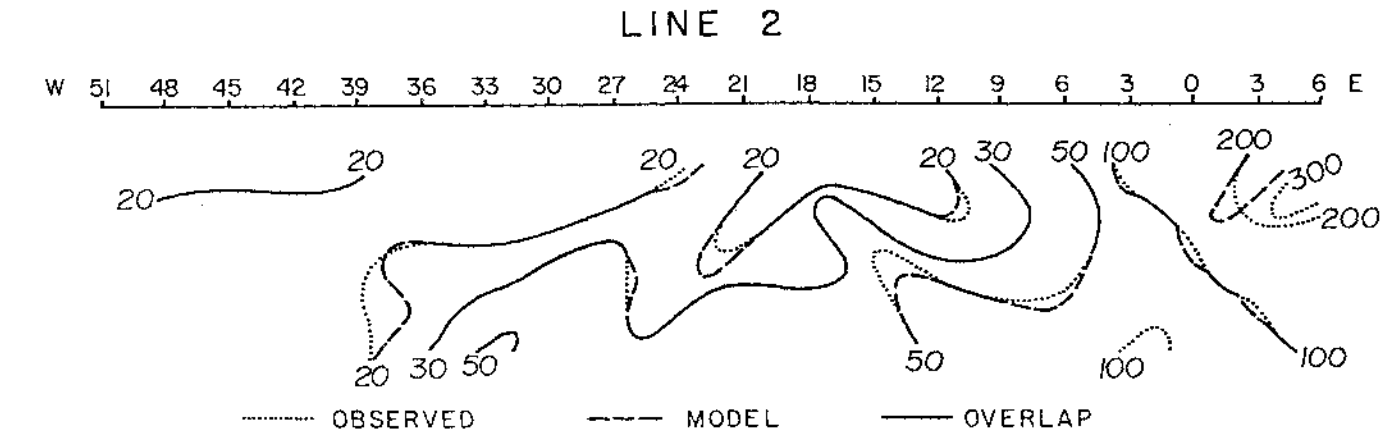
LINE 2
W 51 48 45 42 39 36 33 30 27 24 21 18 15 12 9 6 3 0 3 6 E
20
20
20
20
20
30
50
100
200
300
200
20
30
50
50
100
100
OBSERVED
MODEL
OVERLAP

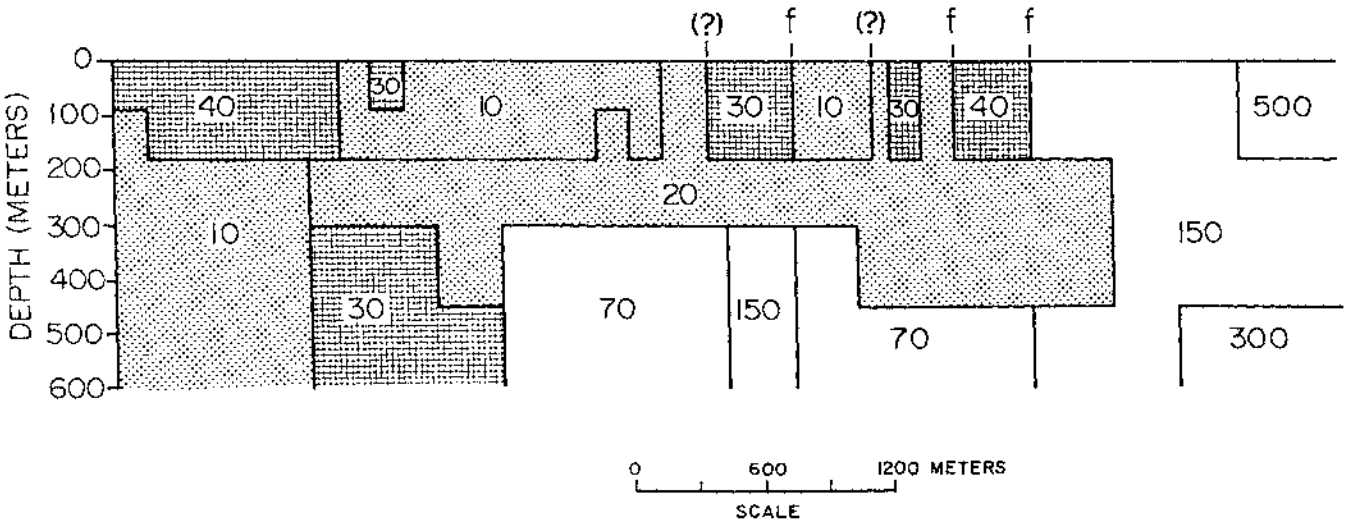
2-D RESISTIVITY MODEL
(?)
f
(?)
f
f
DEPTH (METERS)
0
100
200
300
400
500
600
40
30
10
30
10
30
40
500
10
20
150
30
70
150
70
300
0
600
1200 METERS
SCALE

Fig. 9

modeled resistivity contrasts between stations 3 East and 18 West in Figure 8 coincide with the faults crossing Line 1 in Figure 10. The Opal Mound Fault is located at station 12 West along Line 1 (Figures 1, 10, and 8).

Soil sample analyses (Capuano and Bamford, 1978; Bamford et al, 1980) indicate a possible fault passing through the area near well 72-16 and station 6 West of Line 1 (Figure 10). The modeled resistivity data (Figure 8) also suggest a fault; the 300m dipole data show a contrast of 12 to 50Ω-m at station 6 West.

Figure 9 shows the resistivity model for Line 2. The majority of the computed resistivities were within 10% of the observed resistivities. The surface locations of the modeled resistivity contrasts marked "f" correspond to faults crossing Line 2 in Figure 10. Dashed lines in Figure 10 are inferred faults and correspond to the resistivity contrasts marked by "?" in Figure 9.

Figures 8 and 9 show high resistivities on the eastern parts of the survey lines near the Mineral Mountains, with a transition to lower resistivities toward the west. The zones of low resistivity modeled in both lines over the geothermal system extend westward beneath more resistive material. A likely geological explanation for this is that brine is leaking from the convective hydrothermal system westward beneath the valley sediments. At station 39 of Line 2 in Figure 9, the resistive over conductive regime changes to a conductive over resistive regime. We assessed the character and magnitude of phase shifts due to coupling over these two regimes by calculating the one-dimensional EM coupling for the dipole-dipole array (Hohmann, 1973). Figure 11 shows

FIG. 10. Fault pattern in survey area based on geological evidence (Nielson et al, 1979). Solid lines indicate faults verified in the field; dashed lines indicate inferred faults. Relative fault movement marked by U, D. Shaded area is Mineral Mountains; white area is alluvium; black areas are altered rocks and sinter deposits. Producing wells shown by solid dots, "dry wells" by open circles, shallow alteration holes by circles with crosses.

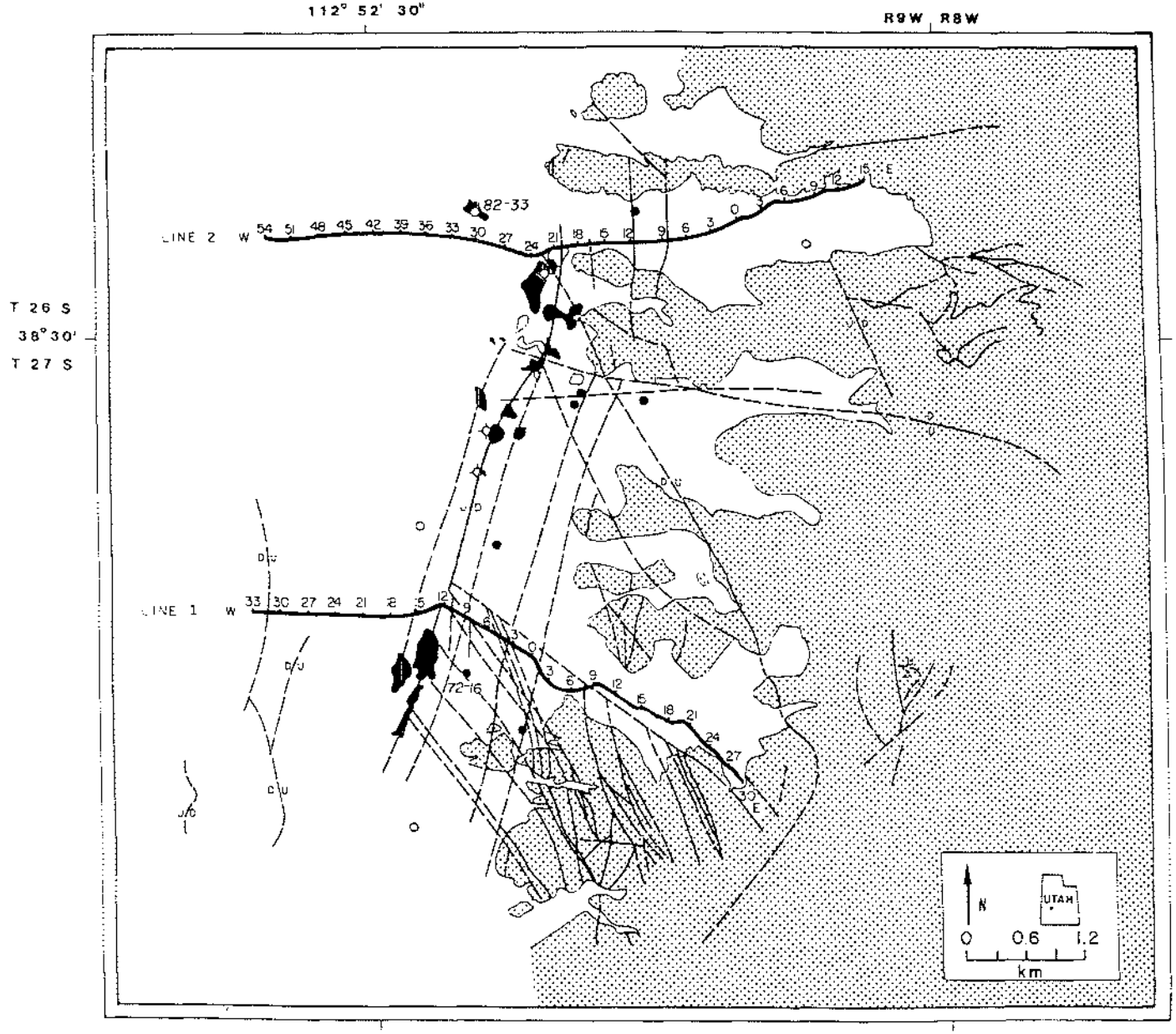
112° 52' 30"
R9W R8W
T 26 S
38°30'
T 27 S
LINE 2 W
LINE 1 W
82-33
72-16
N
UTAH
0 0.6 1.2
km

CHW
Fig. 10

FIG. 11. 1D electromagnetic coupling for two different earth models shown for dipole-dipole array n spacings of 1, 3, and 5. Solid lines are for resistive over conductive model; dashed lines are for conductive over resistive model. Depth to interface = 180 m.

CHU
Fig. 11

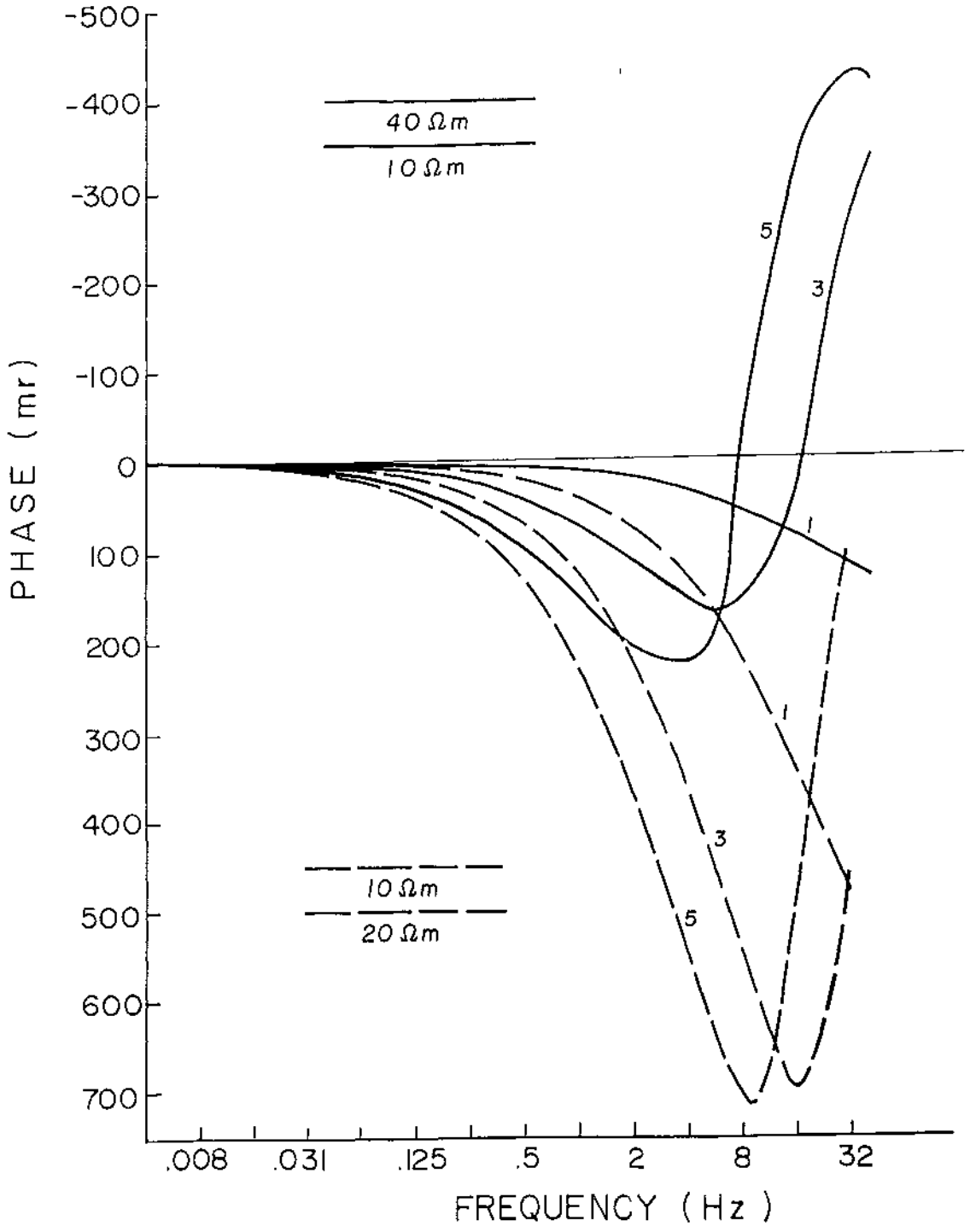
-500
-400
-300
-200
-100
0
100
200
300
400
500
600
700
PHASE (mr)
40 Ωm
10 Ωm
10 Ωm
20 Ωm
5
3
1
1
3
5
.008
.031
.125
.5
2
8
32
FREQUENCY (Hz)

the coupling calculations. Negative phase values are obtained above 4Hz for n spacings greater than 1 for the resistive over conductive model. In contrast, all coupling phase values are positive for the conductive over resistive model, for the range of frequencies and n spacings used in the field measurements. Comparing these coupling calculations with the phase pseudosections from Line 1 in Figures 7a-7c, we see that the field phase data on either side of the modeled contact at 39 West agree in every aspect with the behavior of the coupling curves in Figure 11. Away from the contact, the magnitude of the coupling indicated by the theoretical curves is in good agreement with the observed data at each frequency. The good agreement of the theoretical coupling and the observed phase data strengthens the resistivity interpretation on the western portion of Line 2.

Interpretation of the IP responses in our phase data from the Roosevelt Hot Springs thermal area is hindered by telluric noise below 1/16Hz. If we avoid telluric noise by utilizing the measurements obtained at 1/16Hz and above, then EM coupling must be removed from the field data. Techniques to remove EM coupling from field data were not published until 1974, when Hallof proposed a method based on "phase extrapolation". Since then, two other methods have been suggested, one which is proprietary (Wynn and Zonge, 1975, 1977), and one which involves inversion to Cole-Cole models (Pelton et al, 1978). Coupling removal was attempted using phase extrapolation.

Phase extrapolation. - Hallof (1974) proposed fitting phase data, taken between 0.05Hz and 1.25Hz, with a linear or quadratic function. Extrapolating this function to zero frequency leaves the constant term

of the polynomial, which is taken as the IP response. Coupling is removed when the interpolated data are accurate if, over the bandwidth of the fit, the IP response is constant while the frequency dependence of the polynomial adequately describes that of the coupling. As a reasonable compromise between the effects of telluric noise and EM coupling we chose the frequencies 1Hz, 1/4Hz and 1/16Hz. Since the laboratory data of Figures 2a-2f showed slowly varying IP phases at these frequencies, we attempted to estimate the IP response in the field data over this band with the phase extrapolation technique.

The phase data from Lines 1 and 2 were fitted with a quadratic polynomial at 1Hz, 1/4Hz and 1/16Hz. The pseudosections obtained using the constant terms of the quadratic fits are shown in Figure 12. In both lines, the residual phases obtained over the geothermal system lie within the range of values obtained from the low frequency laboratory measurements, except for the region beneath stations 27 and 30 West on Line 2. At this location, a metal pipeline crosses the survey line at an angle of about 25 degrees, and may cause spurious IP effects (Nelson, 1977). In addition, the pipeline leads to the reinjection well 82-33 (Figures 1 and 10), located approximately 150m north of station 30 West. This well reaches a depth of 1892m and is cased with metal (Lenzer et al, 1976). Campbell (1977) reported IP anomalies due to drill hole casings in an area containing 64 metal cased holes, 100m apart.

There is a suggestion that the 100m data on Line 1 might be outlining the top of a weakly responding zone (10mr). The spacial extent of this region is similar to the most conductive unit (7Ω-m) in

FIG. 12. Pseudosections resulting from extrapolation of 1Hz, 1/4Hz, and 1/16Hz phase data from Lines 1 and 2. Phase values for Line 1, a = 100 m, fit into the bottom pseudosection as shown. Dotted contours of the top pseudosection outline areas with negative phase values.

CHU
Fig. 12

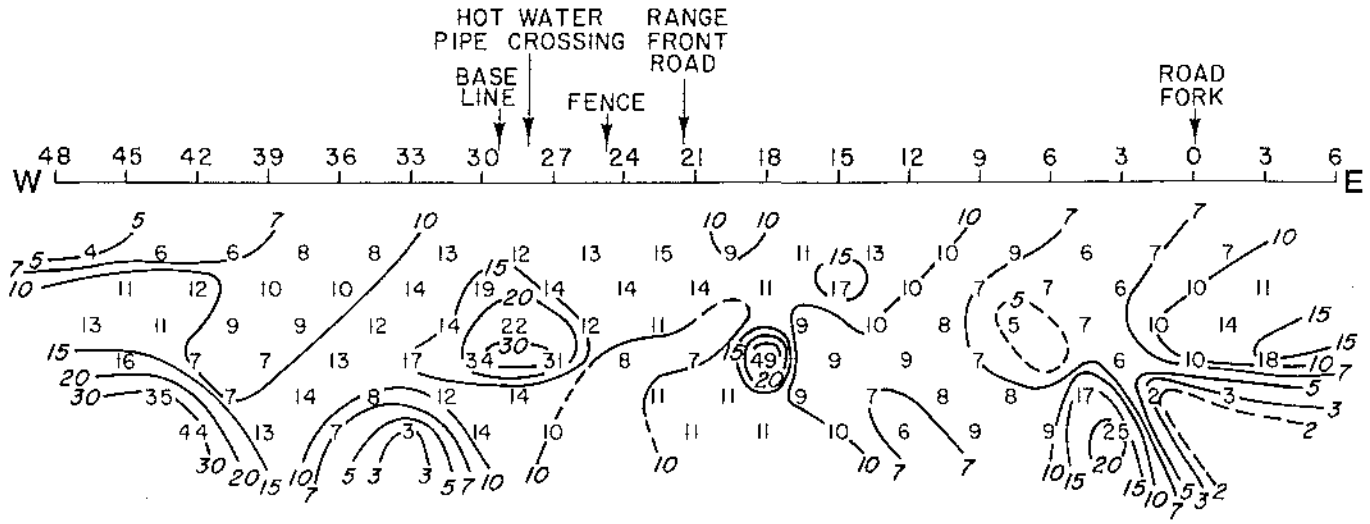

LINE 2 a=300m

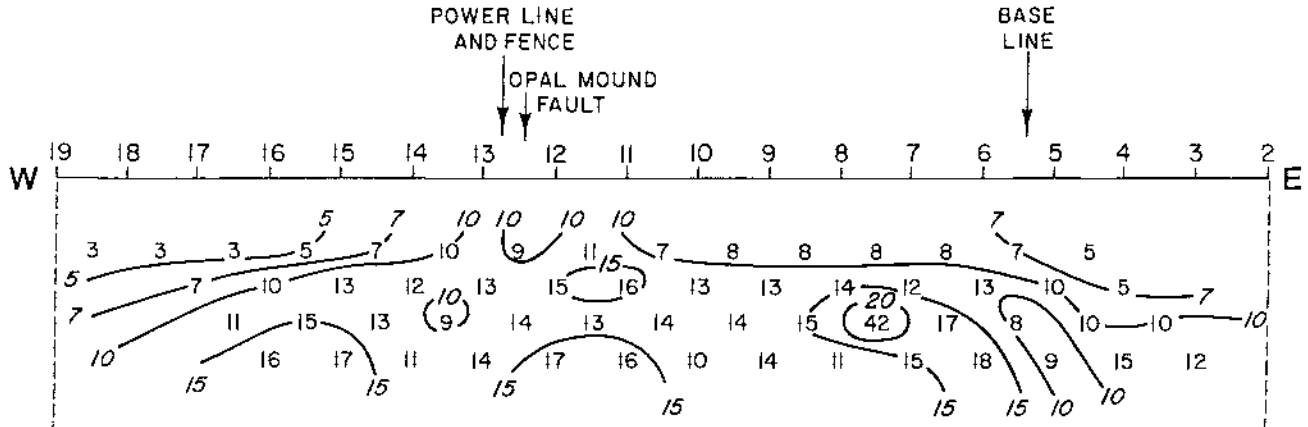

LINE 1 a=100m

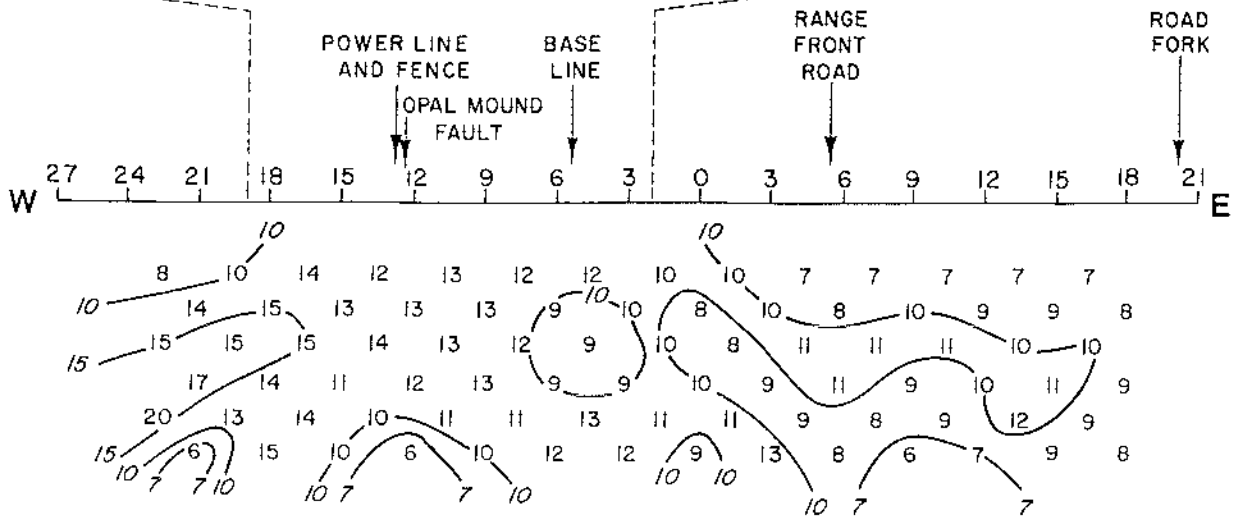

LINE 1 a=300m

the model of Figure 8.

A comparison of the phase extrapolated data shows some general similarities to the original data at 1/16Hz, although the extrapolated phases are somewhat smaller. This probably indicates that at this frequency the EM coupling is less than the true IP effects.

The phase extrapolation technique gives an estimate of the minimum IP response in the frequency band of the quadratic fit. Unfortunately, host rocks surrounding the geothermal area also exhibit approximately the same magnitude of polarization, if the phase extrapolation is correct. Hence, this particular geothermal system is not well delineated by its IP response between 1/16Hz and 1Hz.

Changes in background resistivity, percentages of polarizable materials, grain size, or range of grain sizes can each produce changes in the frequency dependence of the IP effect. It is possible that hydrothermal alteration could produce changes in these parameters which would cause systematic variations in the frequency dependence of the IP response and thus delineate the geothermal area. However, more sophisticated coupling removal must be effected if the frequency dependence of the IP response in the data is to be examined.

SUMMARY AND CONCLUSIONS

The laboratory research on the contribution of pyrite or marcasite and clays to the IP effect has resulted in a number of empirical findings:

(i) our hydrothermally altered rock samples do exhibit IP behavior: at 1/256 Hz, the IP effect is small, from 3 to 23 mr; at 1024 Hz, IP phase values ranged from 20 to 100 mr,

(ii) the IP effect is frequency dependent, even to the lowest frequencies,

(iii) the resistivity of our samples is affected by temperature and the presence of clays; the resistive behavior fits either Archie's Law or the Waxman-Smits model, depending upon the clay content,

(iv) the IP effect is not affected markedly by moderate changes in temperature for the frequency range 1/256 Hz to 1024 Hz, and

(v) the IP behavior is affected by the presence of pyrite, and of clay minerals, the effect of pyrite appearing to differ from that of polarizable clay: for the frequency range of 1/4 Hz to 1024 Hz, pyrite tended to increase the phase values, while clay tended to decrease the phase values.

If we assume that the IP behavior of the rock core sample is determined solely by the presence of polarizable clay and/or pyrite, and

that the principles illustrated in Figure 3, discovered through the study of synthetic ore samples, hold for any polarizable particle, then we can add these inferences:

(vi) pyrite affects the phase spectrum well above 1 Hz; the peaks of the phase dispersions associated with pyrite and clay are above 10^3 Hz,

(vii) the maximum value of the phase dispersions associated with pyrite is at lower frequency than that of clay; this is due mainly to the difference in grain size between the mineral groups,

(viii) the dispersions of clay and pyrite superimpose to explain the IP effect, and

(ix) the manner in which the dispersions of clay and pyrite contribute to the final phase spectrum of the core sample depends upon the relative positions of these two dispersion curves along the frequency axis, as well as the shape and magnitude of each of the dispersion curves; all of these factors are a function of several parameters, including the resistivity of the rock, the amount of polarizable material present, and the grain sizes of the particles causing the IP effect.

On the basis of these hypotheses, we suggest that our uncoupled field data are low frequency asymptotes of many superposed spectral dispersions whose main peaks are well above the range of frequencies used in the field.

In conclusion, we note that there is good agreement between the phase extrapolated field data and the laboratory results. The IP

response of this hot-water dominated system is generally small, in the range of 7 to 15 mr. The field and laboratory data also indicate that IP responses of from 20 to 34 mr are possible, though infrequent. There is no large scale delineation of the geothermal field. However, it is important to note that the zone of maximum alteration was not sampled by the two IP traverses documented here.

ACKNOWLEDGEMENTS

This research was funded by the Department of Energy, Division of Geothermal Energy, Contract DE-AC03-79ET27002. Thanks are due to Dr. W. T. Parry, for his aid in assessing the CEC values by atomic absorption spectrometry.

REFERENCES

Ballantyne, G. H., 1978, Hydrothermal alteration at the Roosevelt Hot Springs thermal area, Utah: characterization of rock types and alteration in Getty Oil Company well Utah State 52-21: Topical rep., v. 78-1701.a.1.1.4, DOE/DGE contract EG-78-C-07-1701, Univ. of Utah, 24 p.

Ballantyne, J. M., and Parry, W. T., 1978, Hydrothermal alteration at the Roosevelt Hot Springs thermal area, Utah: petrographic characterization of the alteration to 2 kilometers depth: Tech. rep., v. 78-1701-a.1.1, DOE/DGE contract EG-78-C-07-1701, Univ. of Utah, 26 p.

Bamford, R. W., Christensen, O. D., and Capuano, R. M., 1980, Multi-element geochemistry of solid materials in geothermal systems and its applications, Part 1: The hot-water system at the Roosevelt Hot Springs KGRA, Utah: Univ. Utah Research Inst., Earth Science Laboratory, report no. 30, DOE/DGE Contract no. DE-AC03-79ET-27002, 168 p.

Campbell, R. E., 1977, Geophysical drill hole casing anomalies, in Workshop on Mining Geophysics: S. H. Ward, ed., University of Utah, Dept.of Geol. and Geoph.

Capuano, R. M., and Bamford, R. W., 1978, Initial investigation of soil mercury geochemistry as an aid to drill site selection in geothermal systems: Univ. Utah Research Inst., Earth Science Laboratory, report no. 13, DOE/DGE Contract no. EG-78-C-07-1701, 32 p.

Chu, J. J., Sill, W. R., and Ward, S. H., 1979, Induced polarization measurements at Roosevelt Hot Springs Thermal Area, Utah: Topical rep., v. 78-1701.a.2.4.1, DOE/DGE contract DE-AC07-78-ET28392, Univ. of Utah, 34 p.

DeWitt, G. W., 1978, Parametric studies of induced polarization spectra: M.S. Thesis, University of Utah, Salt Lake City, Utah.

Dey, A., and Morrison, H. F., 1973, Electromagnetic coupling in frequency and time-domain induced-polarization surveys over a multilayered earth: Geophysics, v. 38, p. 380-405.

Fox, R. C., Hohmann, G. W., Killpack, T. J., and Rijo, L., 1980, Topographic effects in resistivity and induced-polarization surveys: Geophysics, v. 45, p. 75-93.

Grim, R. E., 1968, Clay mineralogy: New York, McGraw-Hill Book Co., Inc.

Hallof, P. G., 1974, The IP phase measurement and inductive coupling: Geophysics, v. 39, p. 650-665.

Hallof, P. G., Cartwright, P. A., and Pelton, W. H., 1979, The use of the Phoenix IPV-2 Phase IP Receiver for discrimination between sulphides and graphite: Presented at the 49th Annual International SEG Meeting, New Orleans, La., November 6.

Hohmann, G. W., 1973, Electromagnetic coupling between grounded wires at the surface of a two-layer earth: Geophysics, v. 38, p. 854-863.

Keller, G. V., and Frischknecht, F. C., 1966, Electrical methods in geophysical prospecting: New York, Pergamon Press.

Killpack, T. J., and Hohmann, G. W., 1979, Interactive dipole-dipole resistivity and IP modeling of arbitrary two-dimensional structures (IP2D users guide and documentation): Univ. Utah Research Inst., Earth Science Laboratory, report no. 15, DOE/DGE Contract no. EG-78-C-07-1701, 107 p.

Lenzer, R. C., Crosby, G. W., and Berge, C. W., 1976, Geothermal exploration of Roosevelt KGRA, Utah (abs.): 17th U.S. Symp. on Rock Mechanics.

Millett, F. B., 1967, Electromagnetic coupling of collinear dipoles on a uniform half-space, in Mining geophysics: Vol. II, Tulsa, SEG.

Nelson, P. H., 1977, Induced-polarization effects from grounded structures: Geophysics, v. 42, p. 1241-1253.

Nielson, D. L., Sibbett, B. S., and McKinney, D. B., 1979, Geology and structural control of the geothermal system at Roosevelt Hot Springs KGRA, Beaver County, Utah (abs.): AAPG Bull., v. 63/5, p. 836.

Nielson, D. L., Sibbett, B. S., McKinney, D. B., Hulen, J. B., Moore, J. N., and Samberg, S. M., 1978, Geology of Roosevelt Hot Springs KGRA, Beaver County, Utah: Univ. Utah Research Inst., Earth Science Laboratory, report no. 12, DOE/DGE Contract no. EG-78-C-07-1701, 120 p.

Parry, W. T., Bryant, N. L., Dedolph, R. E., Ballantyne, J. M., Ballantyne, G. H., Rhors, D. T., and Mason, J. L., 1978, Hydrothermal alteration at the Roosevelt Hot Springs thermal area, Utah: Final rep., v. 78-1701.a.1.1, DOE/DGE contract EG-78-C-07-1701, Univ. of Utah, 29 p.

Parry, W. T., Ballantyne, J. M., Bryant, N. L., and Dedolph, R. E., 1980, Geochemistry of hydrothermal alteration at the Roosevelt Hot Springs thermal area, Utah: Geochim. et Cosmochim. Acta, v. 44, p. 95-102.

Pelton, W. H., Ward, S. H., Hallof, P. G., Sill, W. R., and Nelson, P. H., 1978, Mineral discrimination and removal of inductive coupling with multifrequency IP: Geophysics, v. 43, p. 588-609.

Rijo, L., 1977, Modeling of electric and electromagnetic data: Ph.D. thesis, Univ. of Utah, Salt Lake City, Utah.

Risk, G. F., 1975, Monitoring the boundary of the Broadlands geothermal field, New Zealand: Second UN Symposium on the Development and Use of Geothermal Resources, San Francisco, Proceedings, v. 2, p. 1185-1189.

Rohrs, D., and Parry, W. T., 1978, Hydrothermal alteration at the Roosevelt Hot Springs thermal area, Utah: Thermal Power Company well Utah STate 72-16: Topical rep., v. 78-1701.a.1.1.3, DOE/DGE contract EG-78-C-07-1701, Univ. of Utah, 23 p.

Ross, H. P., 1979, Numerical modeling and interpretation of dipole-dipole resistivity and IP profiles, Cove Fort-Sulphurdale KGRA, Utah: Univ. Utah Research Inst., Earth Science Laboratory, report no. 26, DOE/DGE Contract no. EG-78-C-07-1701, 22 p.

Seigel, H. O., 1959, Mathematical formulation and type curves for induced polarization: Geophysics, v. 24, p. 547-565.

Sill, W. R., and Bodell, J., 1977, Thermal gradients and heat flow at Roosevelt Hot Springs: Tech. rep., v. 77-3, DOE/DGE contract EY-76-S-07-1601, Univ. of Utah, 63 p.

Tripp, A. C., 1977, Rock conduction mechanisms at Roosevelt Hot Springs KGRA, Appendix D: in Electromagnetic and Schlumberger resistivity sounding in the Roosevelt Hot Springs KGRA: M.S. Thesis, University of Utah, p. 94-107.

Van Voorhis, G. D., Nelson, P. H., and Drake, T. L., 1973, Complex resistivity spectra of porphyry copper mineralization: Geophysics, v. 38, p. 49-60.

Ward, S. H., Parry, W. T., Nash, W. P., Sill, W. R., Cook, K. L., Smith, R. B., Chapman, D. S., Brown, F. H., Whelan, J. A., and Bowman, J. R., 1978, A summary of the geology, geochemistry, and geophysics of the Roosevelt Hot Springs thermal area, Utah: Geophysics, v. 43, p. 1515-1542.

Ward, S. H., and Sill, W. R., 1976, Dipole-dipole resistivity surveys, Roosevelt Hot Springs KGRA: NSF final rep., v. 2, grant GI-43741, Univ. of Utah, 29 p.

Waxman, N. H., and Smits, L. J. M., 1968, Electrical conductivities in oil-bearing shaly sands: Trans. Soc. Pet. Eng., v. 243, p. 107-122.

Waxman, M. H., and Thomas, E. C., 1974, Electrical conductivities in shaly sands - I. The relation between hydrocarbon saturation and resistivity index; II. The temperature coefficient of electrical conductivity: Jour. Petroleum Technology, v. 26, p. 213-225.

Wong, J., 1979, An electrical model of the induced polarization phenomenon in disseminated sulphide ores: Geophysics, vol. 44, p. 1245-1265.

Wynn, J. C., and Zonge, K. L., 1975, EM coupling, its intrinsic value, its removal and the cultural coupling problem: Geophysics, v. 40, p. 831-850.

_____, 1977, Electromagnetic coupling: Geoph. Prosp., v. 25, p. 29-51.

Zohdy, A. A. R., Anderson, L. A., and Muffler, L. J. P., 1973, Resistivity, self-potential, and induced-polarization surveys of a vapor-dominated geothermal system: Geophysics, v. 38, p. 1130-1144.

generator unit. To reduce electrode noise, copper sulfate pots were used as potential electrodes for the 300m dipoles. The current transmitted ranged from 4 to 14 amps.

Complex resistivity measurements were taken at eight frequencies from 32Hz down to 1/256Hz. Measurements are presented as magnitude of apparent resistivity (Ω-m), and phase (mr), with the convention that phase lags are positive. A complete set of data collected over Lines 1 and 2 is given by Chu et al, 1979. Representative data are presented here.

Figures 6a,6b show apparent resistivity pseudosections from Line 2 at (a) 32Hz, and (b) 1/64Hz. Apparent resistivities in Figure 6b range from about 300Ω-m near the Mineral Mountains on the east to less than 10Ω-m in the alluvium filled Milford Valley on the west. The apparent resistivity contours of Figure 6b were established at approximately 1Hz and remained unchanged down to 1/256Hz, the lowest frequency measured.

Figures 7a-7c show the phase pseudosections from Line 2 at (a) 32Hz, (b) 1Hz, and (c) 1/64Hz. Maximum phase measurements decrease from about 1000mr for large n spacings at 32Hz (Figure 7a), to between 20 and 30mr at 1/64Hz (Figure 7c). The dashed contours in the left corner of Figure 7c outline a region where erratic negative phases (not plotted) were obtained during a period of strong telluric activity.

Telluric noise increased sharply with decreasing frequency. The percentage errors in the phase measurements below 1/64Hz were larger than those of the apparent resistivity measurements since, as frequency decreased, the phase of the complex resistivity measurement became

FIGS. 6a,6b. Apparent resistivity (Ω-m) pseudosections for (a) 32 Hz and (b) 1/64 Hz, on Line 2. Schematic at top of Figure 5a shows dipole-dipole datum plotted as a function of distance between current (Tx) and potential (Rx) electrode pairs; n is integer multiple of dipole length a; value plotted at intersection of 45 degree lines (dashed) from centers of current and potential dipoles.

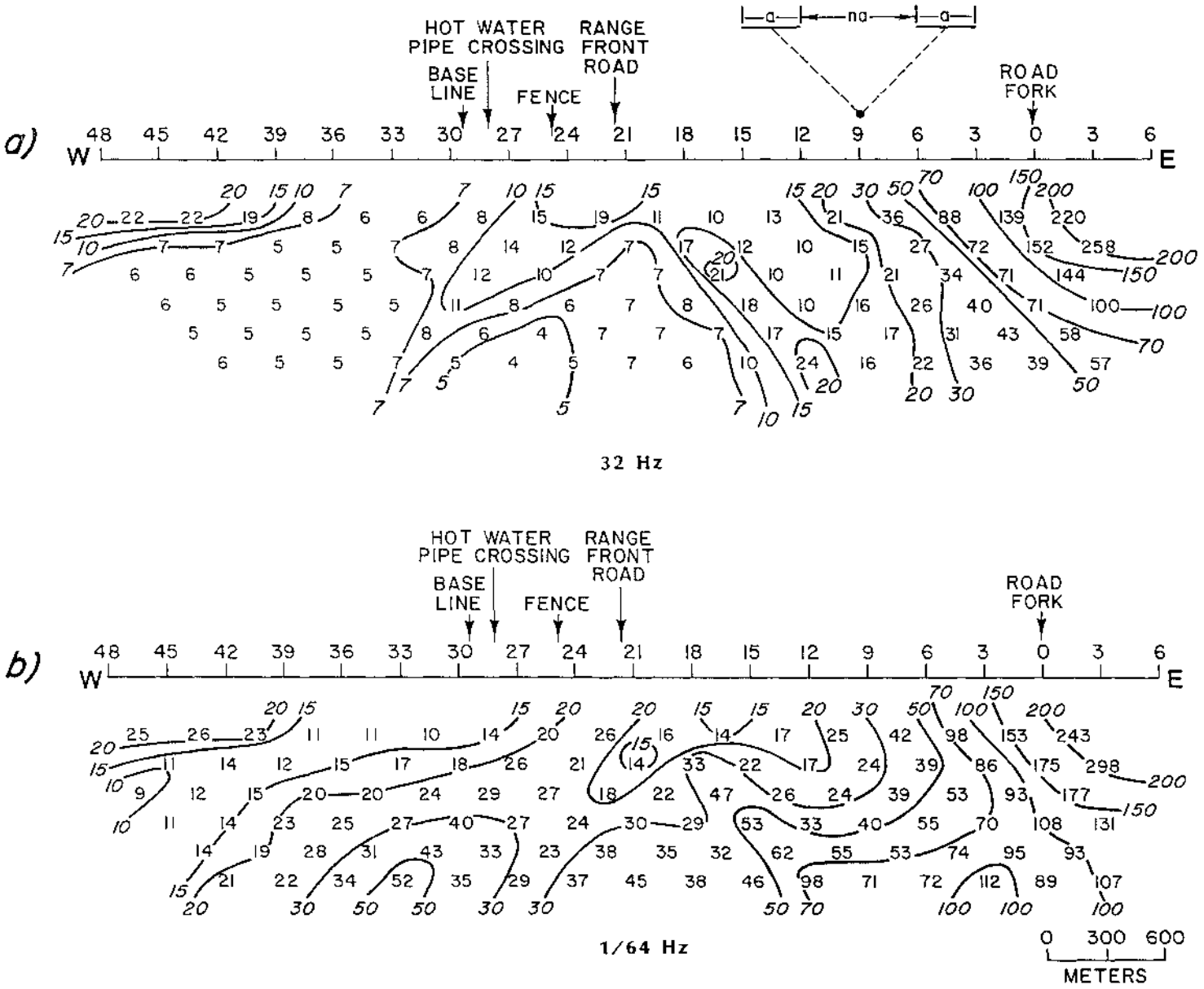

CHU
Figs 6a,6b

FIGS. 7a-7c. Phase (mr) field data from Line 2. Pseudosections for 3 frequencies shown: (a) and (b) are dominated by coupling, while (c) shows influence of telluric noise. Note negative phase data on left side on 32 Hz pseudosection.

CHU
Figs 7a-7c

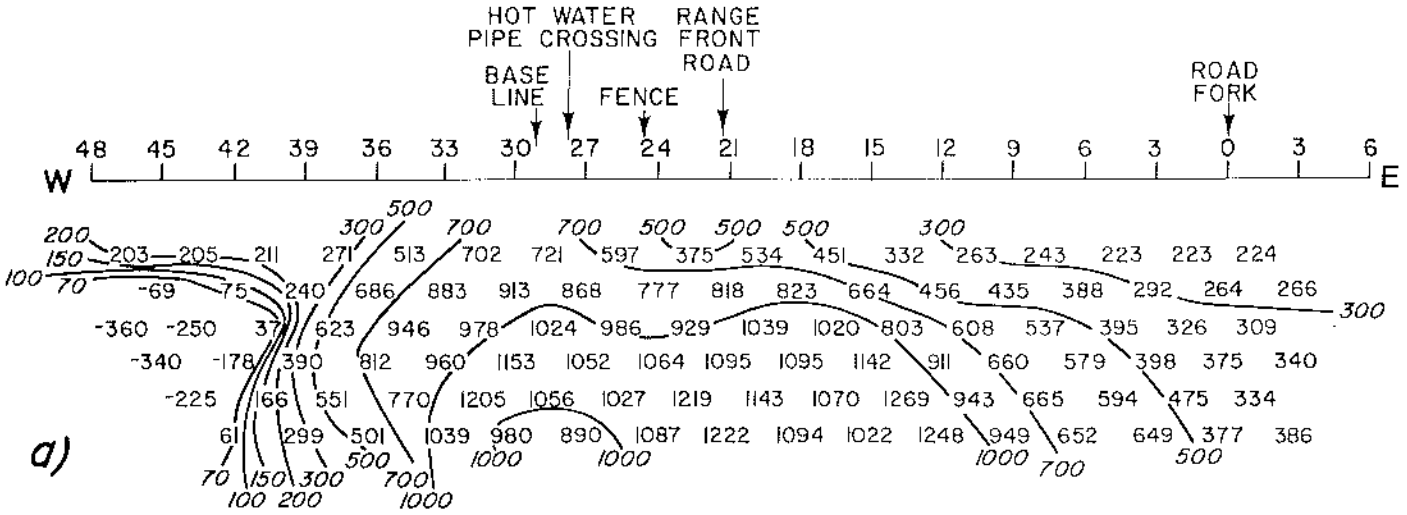

32 Hz

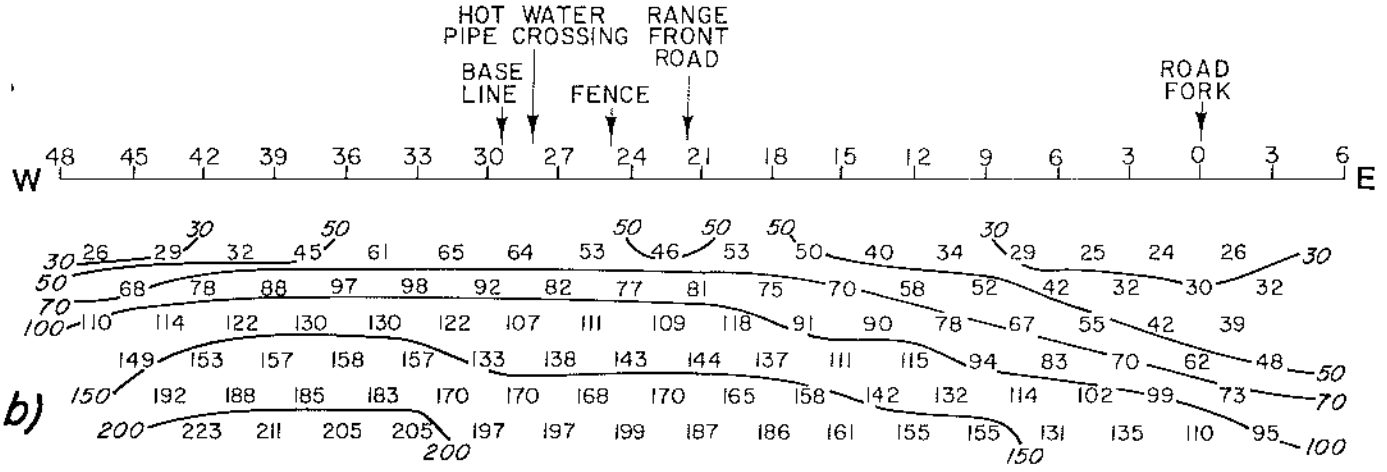

1 Hz

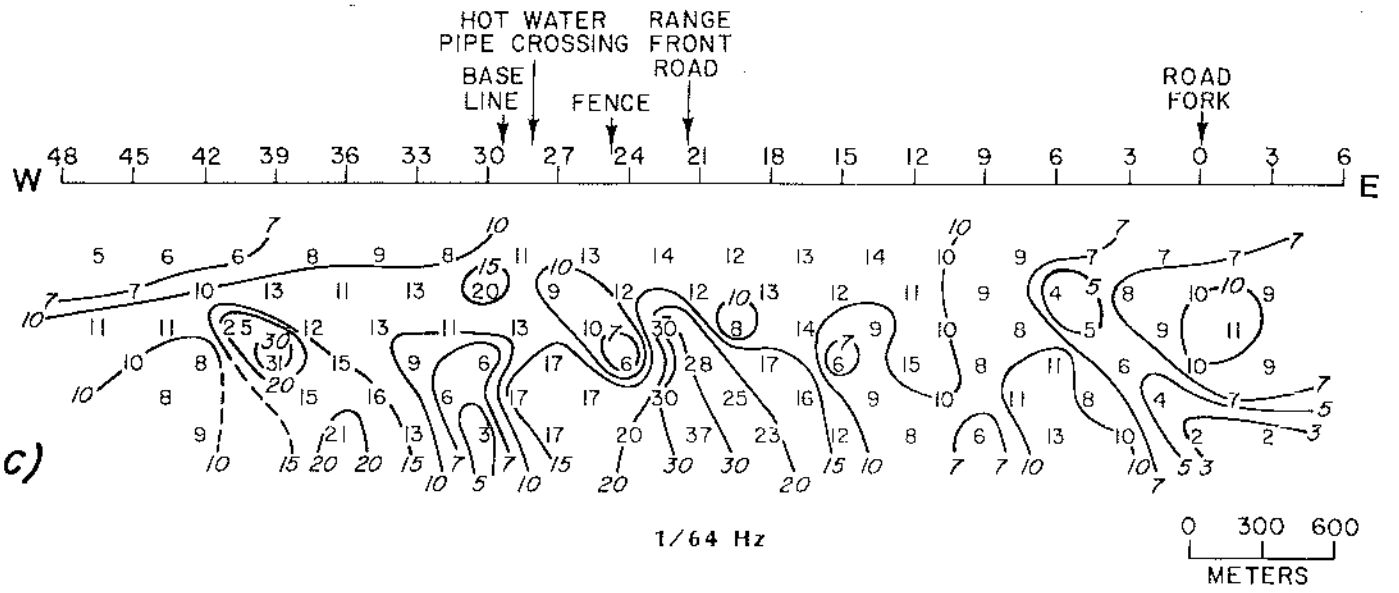

1/64 Hz

smaller (compare Figures 6 and 7). This result is expected when amplitudes and phases are calculated from equally noisy in-phase and quadrature field measurements.

EM coupling severely contaminated the amplitude and phase data above 1 Hz (Figures 6a and 7a). The variation with frequency of both data sets was much more rapid than that observed from the laboratory measurements of IP response for the core samples shown in Figures 2a-2f. The apparent resistivity field data was not severely affected by EM coupling below approximately 1Hz. However, coupling, evaluated as a percentage of the total measurement, affected the phase data to lower frequencies than the apparent resistivity data. In addition, as frequency and EM coupling decreased, the phase data became increasingly contaminated with telluric noise.

Data Interpretation

We modeled the observed resistivity data at 1/256Hz, using a 2D finite-element forward routine initially developed by Rijo (1977), and then modified by Killpack and Hohmann (1979). Topographic effects (Fox et al, 1980) for our survey lines were considered negligible. The resistivity models shown in Figure 8 and 9 are undoubtedly non-unique. This fact must be borne in mind when attempting to interpret the models in a geologic sense.

Figure 8 shows the resistivity model for Line 1, based upon the 100m and 300m dipole-dipole data. The calculated resistivities were within 10% of the observed resistivities for the 100m dipole-dipole data. A less satisfactory fit is shown between computed and observed data values for the 300m dipole data. The surface location of the

FIG. 8. 2D model (bottom) for Line 1. Contoured apparent resistivity data (top) gathered at 1/256 Hz. Solid contours indicate coincidence of modeled (dashed) and observed data (dotted) contours. Fine contour lines and shallow 2D resistivity model between stations 0 and 20 West represent detail obtained with 100 m dipoles. Low (12 Ω-m) and intermediate (30-50 Ω-m) resistivities of model, based on a = 300 m data, shown with dotted and cross-hatched patterns respectively.

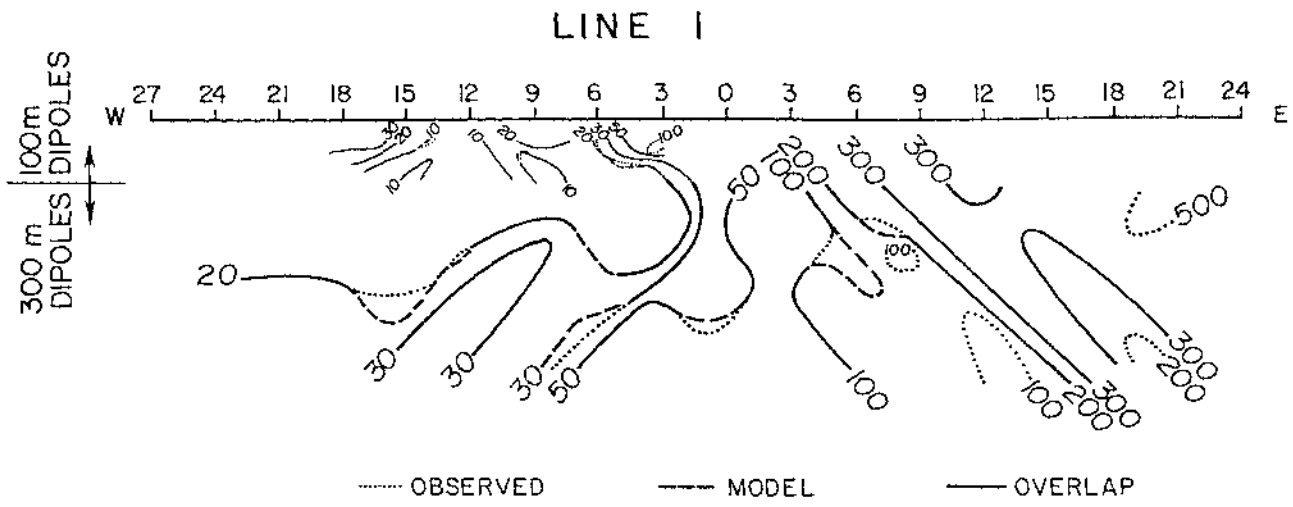
LINE I
100m DIPOLES
300 m DIPOLES
W
27 24 21 18 15 12 9 6 3 0 3 6 9 12 15 18 21 24
E
OBSERVED
MODEL
OVERLAP

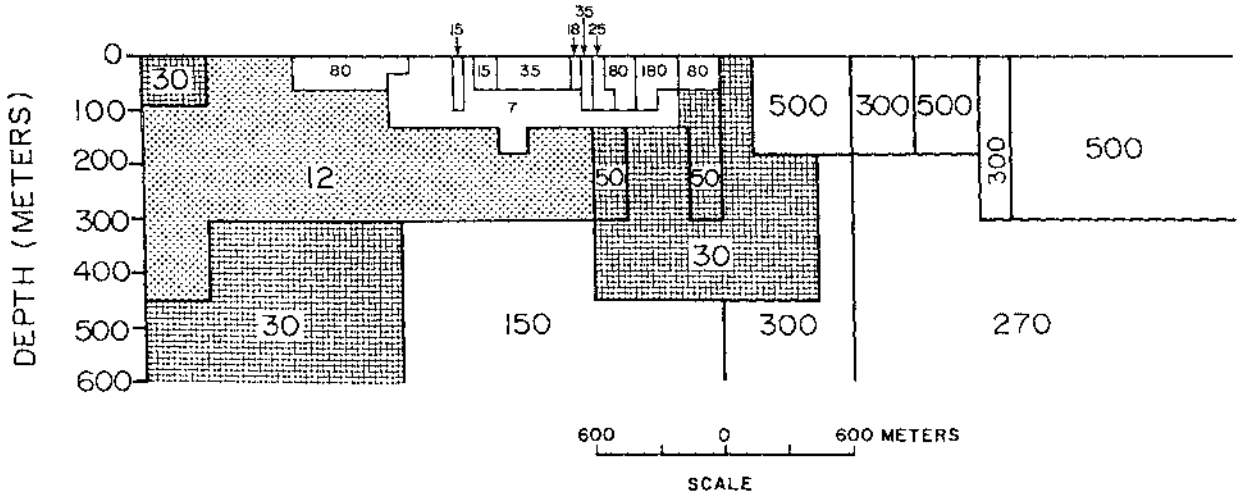
2-D RESISTIVITY MODEL
DEPTH (METERS)
0
100
200
300
400
500
600
30
80
15
35
18
25
7
180
500
300
12
50
150
270
600 0 600 METERS
SCALE

Fig. 8